6

Effect of Mg²⁺ Doping on Formation of Apatite Layer by Bioactive Sol-Gel Glass-Ceramic

K. M. Tohamy, M.M. El-Okr, A.F. Ali[*], Islam E. Soliman and M.I. El-Gohary

Physics Department, Biophysics Branch, Faculty of Science, Al-Azhar University, Nasr City and [*]Inorganic Chemistry Department, National Research Center (NRC), Dokki, Cairo, Egypt.

BIOACTIVE glass–ceramics of mixed alkali and alkali earth were prepared by quick alkali mediated sol–gel method. The influence of varying MgO content substituted for SiO_2 on the structure and thermal behavior of glass compositions in the SiO_2–Na_2O–CaO–P_2O_5–MgO system. This system was investigated by DSC, TGA, XRD and FTIR. In addition, to study *in-vitro* bioactivity of these glass-ceramics were characterized by analysis of apatite-formation layer in simulated body fluid (SBF). The obtained results revealed that at sintering temperature above 900°C, crystallization occurred and glass-ceramics which contain wollastonite, diopside and Calcium phosphate silicate. An increase in concentration of MgO at the expense of SiO_2 led to the formation of diopside in the glass-ceramic. The present results of *in vitro* tests showed that tendency of apatite layer formation decreased with increasing quantity of diopside phase.

Keywords: Sol-gel method, Bioactive glass-ceramic, Diopside, *In-vitro* test.

Since Hench *et al* in 1971s introduced Bioglass®45S5, it has been used as a prosthetic material [1]. The aim of a prosthesis made from a bioactive glass is to guide the growth of new tissue. The glass should therefore activate bone growth but dissolves when the new bone has reached the required strength. Depending on the application, it is often beneficial if the glass can be strengthened by partial crystallization. Up till to now, various types of glass–ceramics have been developed for commercial use, for example, (Ceravital® KGS [2], Cerabone® A-W[3] and Bioverit®[4]). In the last decades, bioactive glass-ceramics attract particular interest for possible clinic applications, because these glass-ceramics provide great possibilities to manipulate their properties, such as transparency, strength, resistance to abrasion, coefficient of thermal expansion and bioactivity[5]. Glass–ceramics have advantages over bioceramics for their convenience in adjustment of mechanical and biomedical properties by controlling heat-treatment processes [6].

Bioactive glass-ceramics are generally regarded as ceramics that are designed to induce specific biological activity for repairing damaged organs. Some bioactive ceramics have already been used to repair bone defects because their bioactivity allows them to achieve tight fixation resulting from direct bonding to living bone due

to a hydroxyapatite layer formed at the surface of the material *in vivo*. At present, various types of bioactive glass-ceramics are under research and development and a great effort is being put into the understanding of the mechanisms and factors governing their properties. For *in vitro* apatite formation, factors such as chemical composition, texture (pore size and volume) and structure are believed to play an important role in the surface interaction of glass-ceramics with the surrounding medium [7].

Sol–gel technique provides an available way to prepare bioactive glasses. Compared with the traditional melting method, the sol–gel procedure is performed at lower temperature and it allows us to obtain glasses with higher purity and homogeneity. Magnesium is an important trace element existing in human body. Enamel, dentin and bone contain 0.44, 1.23 and 0.72 wt% of magnesium, respectively[8]. Moreover, magnesium has been shown to play an important role in bone development and maintenance [9]. The aim of the present work is to study the effect of Mg additive in the prepared sol-gel bioactive glass-ceramics. The different phases with respect to Mg doping quantity were investigated and described for apatite formation by *in-vitro* test, to be applied *in vivo* for treatment of bone fractures.

Materials and Methods

Materials

Tetraethyl orthosilicate (TEOS), calcium nitrate tetrahydrate $Ca(NO)_3 \cdot H_2O$, sodium nitrate $NaNO_3$, magnesium nitrate hexahydrate $Mg(NO_3)_2 \cdot 6H_2O$ and triethyl phosphate (TEP) were all $\geq 98\%$ and were purchased from Buchs Switzerland. Ammonia solution, 33%, and nitric acid, 68%, were purchased from Merck, USA. Both nitric acid and ammonia solutions were diluted to 2 M using distilled water.

Sol–gel synthesis of magnesium-doped bioactive glass

Bioactive glass containing 0, 1,3 and 5 wt% of MgO were synthesized through a quick alkali-mediated sol–gel technique [10,11]. MgO was added to the glass compositions at the expense of SiO_2. Table 1 presented the nominal compositions and codes of the prepared bioactive glass. Initially, tetraethyl ortho-silicate, distilled water and 2M nitric acid (as a hydrolysis catalyst), were successively mixed in ethanol and the mixture was allowed to react for 60 min under continuous magnetic stirring for the acid hydrolysis of TEOS. Then appropriate amounts of series reagents were added in the following sequence: (TEP), $Ca(NO)_3 \cdot H_2O$, $NaNO_3$ and $Mg(NO_3)_2 \cdot 6H_2O$, allowing 30 min for each reagent to reacts completely. After the final addition, mixing was of all reagents continued for 60 min to complete hydrolysis. Ammonia solution of 2M concentration (a gelation catalyst) was dropped into the mixture. The mixture was then agitated with glass rode (like as mechanical stirrer) to prevent the formation of a bulk gel. Finally, each prepared gel was dried at $75^{\circ}C$ for 2 days in a drying oven. According to the results of the thermal analysis of the dry gels, which showed that there was no further weight loss above $600^{\circ}C$, the gels was stabilized by heat treatment, at a constant heating rate of $10^{\circ}C$ min^{-1} up to $600^{\circ}C$. All heating samples sintered at $900^{\circ}C$ to obtain different crystalline phases.

TABLE 1. The nominal compositions and codes of the prepared magnesium doped sol–gel bioactive glasses.

Sample code	Composition				
	SiO$_2$	Na$_2$O	CaO	P$_2$O$_5$	MgO
SPM$_0$	55	5	35	5	0
SPM$_1$	54	5	35	5	1
SPM$_3$	52	5	35	5	3
SPM$_5$	50	5	35	5	5

S (silica), **P** (phosphorus), **M** (magnesium)

Characterization

Thermogravimetric analyses (TGA) and differential calorimetric analyses (DSC) were performed for the dried gels using a computerized SETARAM labsys™ TG-DSC thermal analysis system. Scans were performed in the atmosphere, and in a temperature range of 50–1000 $^{\circ}$C, at a rate of 10°C min^{-1}. The materials were analyzed using aluminum oxide powder as a reference. The phase analysis of the samples was examined by X-ray diffractometer, model BRUKER axs, using Ni-filtered CuKα irradiation at 40 kV and 25 mA. The infrared spectra of the prepared glass were obtained using Fourier transform infrared spectrophotometer (FT-IR) (Model 580, Perkin-Elmer). Each sample used for infrared spectroscopic analysis was prepared according to KBr technique.

In vitro assays in SBF

In vitro assays were performed in a simulated body fluid (SBF), proposed by Kokubo *et al.*[12]. The SBF solution has a composition and concentration similar to those inorganic parts of human plasma. During soaking process, each disc with dimension (radius=0.5cm, thickness=0.2 cm) was soaked into 50 ml SBF contained in a polyethylene bottle. These bottles were covered with a tight lid and placed in thermodynamic incubator (shaking-water bath) at 37°C for different time periods (control 7,15 and 30 days). After being soaked, the powders were rinsed with deionized water and acetone and dried in air at room temperature.

Results and Discussion

Crystallization behavior of glass powder

Thermal analysis

Thermogravimetric analysis (TGA) and differential scanning calorimetric (DSC), analysis curves for SPM$_1$ are shown in Fig. 1. The TGA curve shows three weight losses as samples were heated to 1000°C. Those weight losses appeared at the temperature intervals of 30–130, 130–320 and 320–620°C. The first weight loss is attributed to the removal water which appears as (humidity and physically adsorbed water) from the surface and any the residual alcohol in the pores of the dried gel [13].

This is reflected in the DCS curves of SPM$_1$ as the first large endothermic peak centered at around 130°C [14], as shown in Fig. 1. The second weight loss is reflected in the exothermic peaks centered at around 270 $^{\circ}$C on the DSC curve of SPM$_1$, which

was most likely due to desorption of chemically adsorbed water [15]. This peak comes from the esterification reaction during condensation of Si-OH groups in the sol–gel network structure[16]. The third weight loss shown by the TGA curve of SPM_1 sample was due to the decomposition of nitrates NO_3^- and ammonia. The endothermic peaks centered at around 495°C on the DSC curve of SPM_1 were due to this decomposition[17]. These results confirmed that all residuals could be removed before 700°C. Therefore, the temperature of 600°C was chosen in this study for stabilization of the glass powder. Still on the DSC curve, a final and well-defined, sharp exothermic peak is located at 783°C. This was due to the glass crystallization into glass-ceramic which confirmed with Vallet-Regí *et al.* [18].
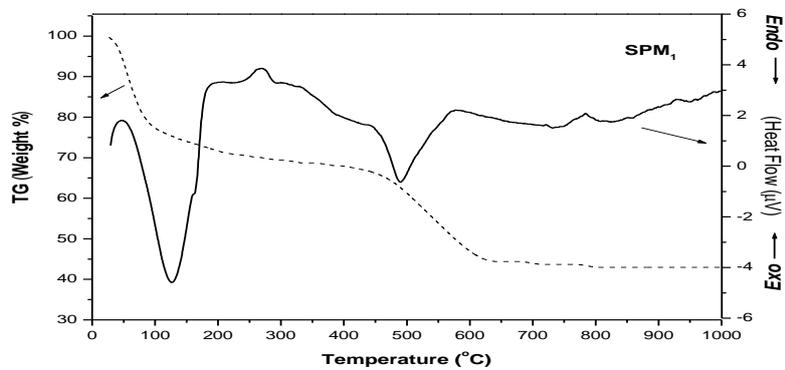

Fig. 1. TGA and DSC curves of the SPM_1 gel powder after 120° C for two days.

X-ray diffraction analysis

Figure 2 Shows the XRD pattern of SPM_1, SPM_3 and SPM_4, where no discernible peaks resulting from lattice periodicity are observed. This confirms that these glasses are amorphous in nature and absence of any crystalline phase after heating at 600°C which characterized by the presence of broad diffraction peak only (amorphous halo) in each glass analyzed [19].
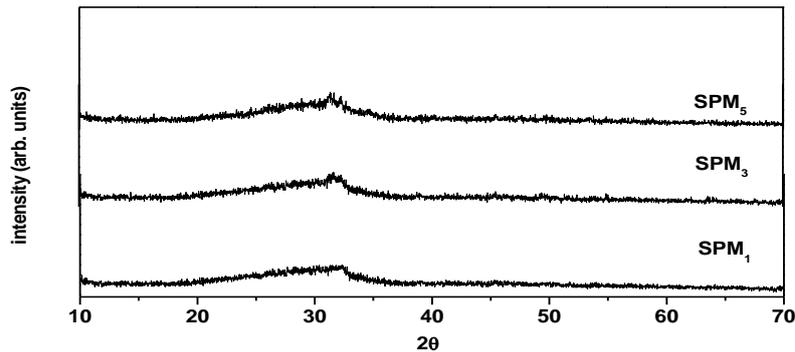

Fig. 2. XRD patterns of the gel glass after annealing at 600 °C for SPM_1, SPM_3 and SPM_5 before soaking in SBF.

All tested gel glass samples were transformed from amorphous to crystal structure after sintering at 900°C and the high degree of crystallization can be observed, while a small amount of a glassy phase is also suggested, as shown in Fig. 3. The crystal states of the tested samples are indicative of the highly internal order and crystalline nature of these materials. For all the tested samples the patterns demonstrate the presence of a mixture of crystalline phases, as shown in Fig. 3.
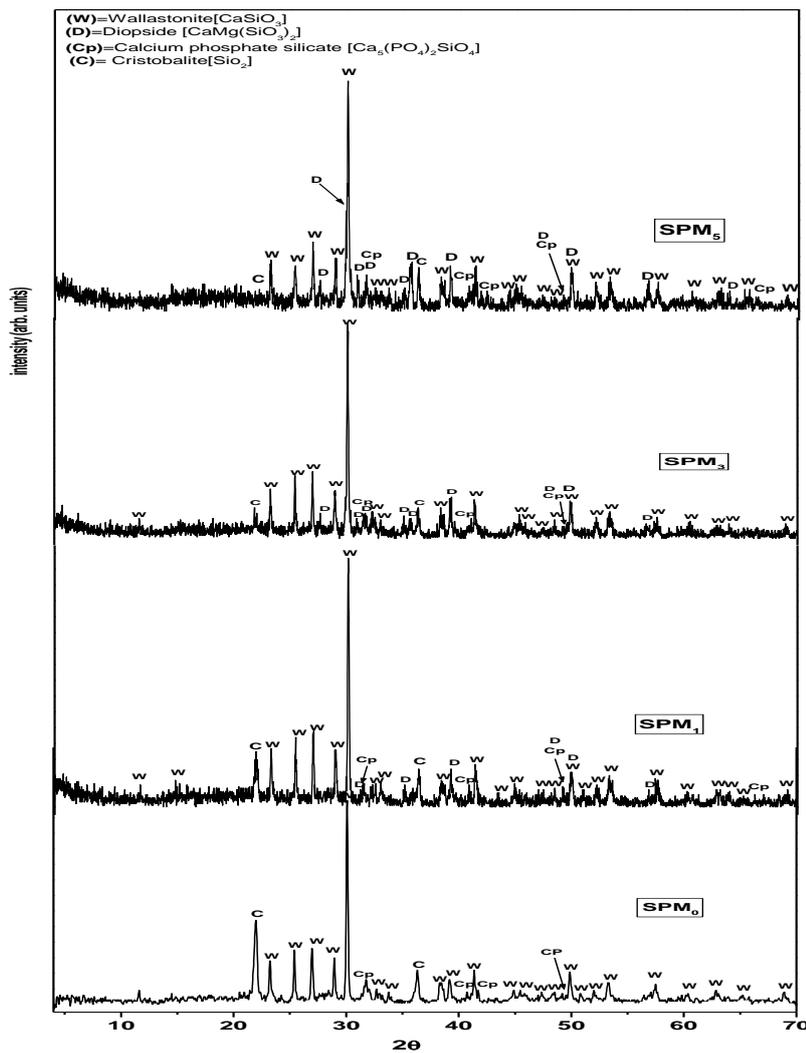

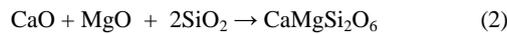**Fig. 3. XRD patterns of SPM₀, SPM₁, SPM₃ and SPM₅ gel glass samples after heat treatment at 900 °C.**

It can be seen that Wollastonite [CaSiO₃] crystal phase predominantly formed because the strong diffraction peaks at 2θ = 23.1, 25.3, 26.8, 28.9 and 30.1 (JCPDS 76-0186) of Wollastonite were detected in XRD patterns for all samples. Diopside [CaMgSiO₆] crystal phase also predominantly formed in SPM₁, SPM₃ and SPM₅ due to the detection of the strong diffraction peaks at 2θ = 27.5, 29.8, 35.5 and 39.2 (JCPDS 75-0945) in XRD patterns.

Besides these two majority phases, the appears of crystalline peaks corresponding to formation of calcium phosphate silicate [Ca₅(PO₄)₂SiO₄] crystal phase with three strongest peaks at 2θ = 31.6, 40.7, 41.1 and 66.2 (JCPDS 73-1181). The last phase is Cristobalite high [SiO₂] phase formed in minor amount with three strongest peaks at (2θ = 21.9, 36.4, 48.4 (JCPDS 76-0934), as shown in Table 2.

TABLE 2. Crystalline phases in various samples.

Samples	Crystalline phases
SPM₀	Wollastonite + Cristobalite high + Calcium phosphate silicate
SPM₁	Wollastonite + Cristobalite high + Calcium phosphate silicate + Diopside*
SPM₃	Wollastonite + Cristobalite high* + Calcium phosphate silicate + Diopside
SPM₅	Wollastonite + Cristobalite high* + Calcium phosphate silicate + Diopside
* Minority phase	

The ability of some cations to build glass forming units or to be housed as modifiers in interstitial positions in the glass structure should also be considered[20]. As we know, Ca²⁺ and Mg²⁺ions present in the glass could combine with the corresponding amount of the remaining silica to form wollastonite and diopside as follows [21]:

$$CaO + SiO_2 \rightarrow CaSiO_3 \qquad (1)$$

$$CaO + MgO + 2SiO_2 \rightarrow CaMgSi_2O_6 \qquad (2)$$

So that, the diopside phase not detected by XRD patterns in sample SPM₀ because of these samples not have amount of MgO content in there composition. This finding is in agreement with that of Salman *et al.* [21] .

FTIR analysis
FTIR spectra taken on the powder SPM₀ sol-gel glass and glass-ceramic after thermal treatment at 900°C for 2hr are shown in Fig. 4. The main absorption bands for the amorphous sol-gel glass are observed at 1050, 960, 760 and 480 cm⁻¹. They are commonly attributed to Si–O–Si and Si–O stretching modes and Si–O–Si bending mode, respectively. These bands are generally observed in amorphous silica glasses for SPM₀ before sintering at 900°C as shown in Fig.4(a) [22].
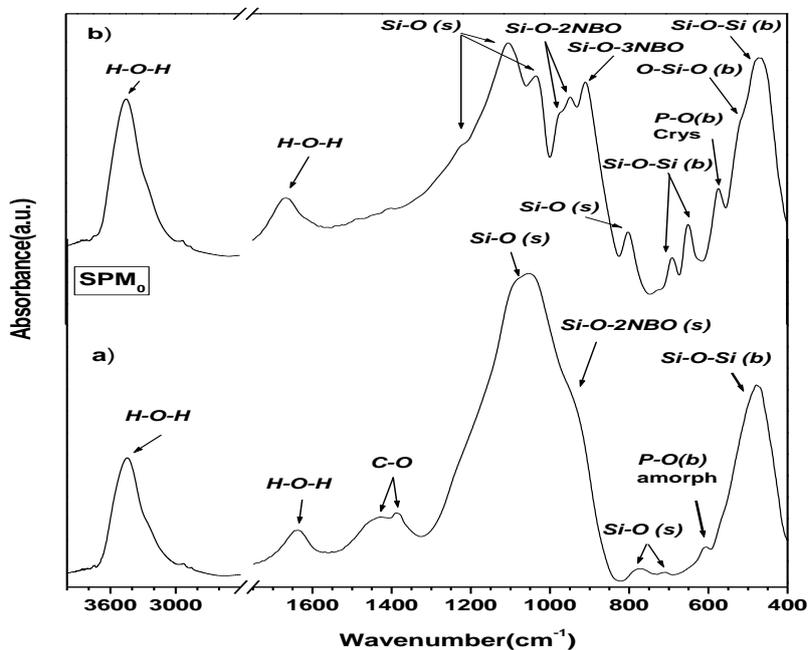
Fig. 4. FTIR spectra of SPM$_0$ (a) before and (b) after thermal treatment at 900 °C for 2 hr.

On the other hand, the FTIR spectra of the powder treated at 900°C shows that the broad band at 1050 cm^{-1} is split into three bands at 1020 cm^{-1}, 1057 cm^{-1},1086 cm^{-1} due to the combination of isolated tetrahedral Si as shown in Fig.4(b). There is also addition new band appeared at around 1200 cm^{-1}, which is assigned to Si–O stretching mode [22]. This band was observed in SPM$_0$ and SPM$_1$ samples.

At the same time, the band at 960 cm^{-1}, which is attributed to the Si–O bond with non-bridging oxygen, also split into three sharp bands at 867 cm^{-1}, 890 cm^{-1} and 935 cm^{-1} and one shoulder at 964 cm^{-1}. The second sharp band assigned to Si-O-3NBO whiles the first, third and shoulder band assigned to Si-O-2NBO[23]. This first band appears at 867 cm^{-1} in the samples that were added magnesium more, SPM$_3$ and SPM$_5$ (as shown in Fig. 4 and 5). Both of them related with Ca^{2+}, Mg^{2+} and Na$^+$ ions in the glass network [24].

Also the two bands at 713 and 761 cm^{-1}, which are assigned to the Si–O–Si bending mode. These two bands appeared with lower wavenumber at 646 cm^{-1} and 683 cm^{-1} with higher intensity which depicts bending vibrational mode in SiO$_4^{-4}$ during mild formation of crystalline silicate phase [25]. At the same time, new absorption band appeared at 792 cm^{-1} which assigned to the Si–O stretching mode. The last band was observed clearly in SPM$_0$ and SPM$_1$ after sintering process.

The absorption band at 480 cm^{-1} corresponds to Si-O-Si and O-Si-O bending modes. This band appears as a broadening peak in sol-gel glass but after thermal treatment the appearance of this band becomes sharper [26] and new shoulder band appears at 515 cm^{-1} which assigned to O-Si-O bending modes, all of them due to the crystallization effects of sol-gel glass. The absorption spectrum of SPM$_0$ sample (as shown in Fig. 4, a) shows small band at 610 cm^{-1}, which corresponds to the amorphous P–O symmetric bending vibration of PO_4^{-3} in phospho-silicate glass. On the other hand, after thermal treatment this phosphate band appears as a highly sharp peak and shifted to lower wavenumber around at 570 cm^{-1} in sample SPM$_0$ after sintering, which called crystal P–O band [27], (as shown in Fig. 4,b). The changes of this band are due to the effects of crystallization process on sol-gel glass and converted it to glass-ceramic. All these bands observed in FTIR spectrum can be attributed to the crystalline phases in glass-ceramic as summarized in Table 3. These results are confirmed with J. Román *et al.,* [28].
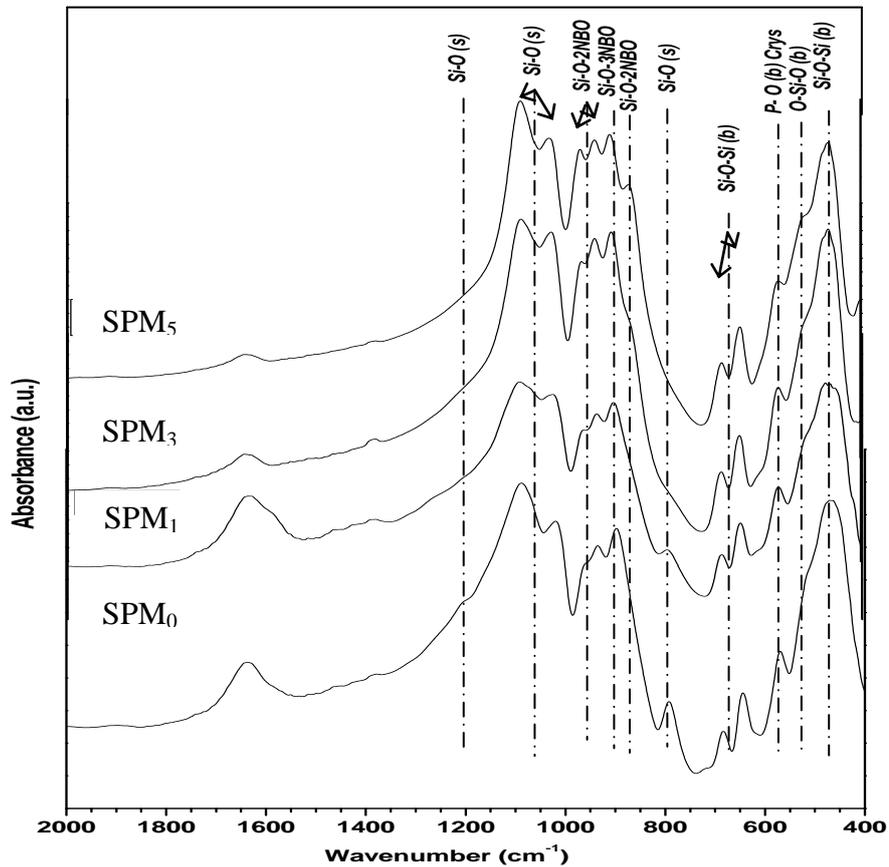

Fig. 5. FTIR spectra for glass-ceramic samples with different additive of MgO content.

TABLE 3. FTIR absorption bands position and their assignment for Glass-Ceramics correspond to crystalline phase. [28-30]

Wavenumber (cm^{-1})	Assignment	Crystalline phase
646, 683, 935, 1020, 1086	Si–O–Si bending Si-O-2NBO Si-O stretching	Wollastonite
792, 1200	Si-O stretching	Cristobalite
570, 489, 515,	P-O bending crystal, Si–O–Si bending, O-Si-O bending,	Calcium phosphate silicate
867, 905-890, 935, 964, 1020	Si-O-2NBO Si-O-3NBO Si-O-2NBO Si-O stretching	Diopside

Effect of magnesium addition on glass-ceramic

From the FTIR absorption spectra of glass-ceramic (Fig. 5), the effects of magnesium addition on the different samples can be determined after heat treatment. It can be seen that, after the first addition of MgO contents in the structure of sol-gel glass composition, the intensity of the absorption bands for Diopside [CaMgSiO$_6$] phase slightly appears after, but the intensity of absorption bands for Wollastonite, Cristobalite and Calcium phosphate silicate phase not affected, as shown in SPM$_1$. As MgO content increased, the intensity of the absorption bands for Diopside (especially bands around at 867 cm^{-1} and 964 cm^{-1}) were appeared with small shoulder and then occurred with strong band as shown in SPM$_5$.

Furthermore, the intensity of the absorption bands for Cristobalite, especially band around at 792 cm^{-1}, were disappeared and the intensity of the absorption band for Wollastonite, especially bands around at 646 and 683 cm^{-1}, weakened. These results clearly revealed that, the increasing amount of MgO in the structure of sol-gel glass causes the formation of groupings (domains) the structure of which changes from the structure of Cristobalite and wollastonite to the structure corresponding to silicate of Diopside [CaMgSiO$_6$] phase. These observations agree with the XRD results as shown in Fig. 3 and confirmed with Szumera *et al.*[28].

bioactivity behavior of glass-ceramic in SBF
XRD analysis

XRD patterns of glass-ceramics after 30 days of soaking in SBF are given in Fig. 6. Besides the original phase of CaSiO$_3$ and CaMgSiO$_6$, the diffraction peaks at 2θ= 25.8°, 31°, 39.3° and 40.8° corresponding to (0 0 2), (2 1 1), (1 3 0) and (1 0 3) reflections of an apatite phase were detected on the XRD pattern of the glass-ceramic. These peak positions of XRD patterns matched well with the standard pattern of apatite card (JCPDF 82-1943).

The results also justify that the relative intensity of the main peak (2 2 0) before soaking in SBF is larger than that of this peak after soaking for all glass-ceramic samples. This result can be attributed to the dissolution of wollastonite ($CaSiO_3$) phase during immersion in SBF for 30 days as shown in Fig. 7. When $CaSiO_3$ ceramic get in the contact with SBF solution, a partially dissolution occurs in the materials network and this partial dissolution produces an ionic exchange between Ca^{2+} and silanol groups on the surface of the ceramic material. These ion exchanges enhance crystallization of nuclei for the Ca–P and the nucleation and growth of the apatite layer proceeds by reaction of ions from the SBF. This is evidenced by appearance of characteristic peaks of apatite phase [31].
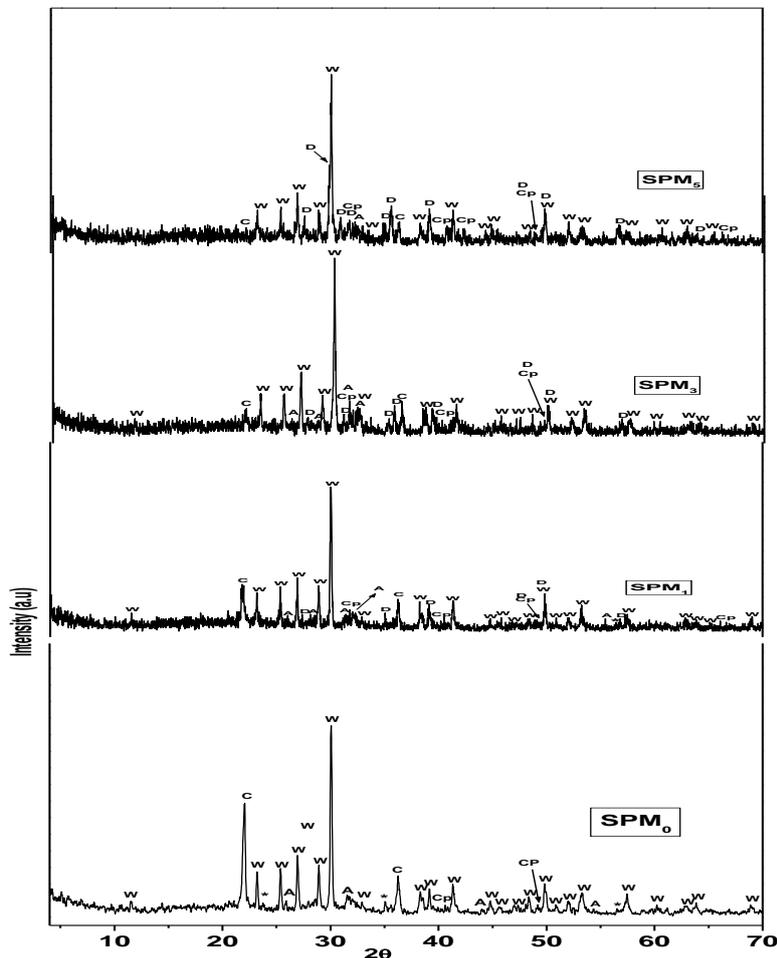

Fig. 6. XRD patterns of glass-ceramic samples after soak in SBF for 30 days, the major peaks of calcite (*), Cristobalite (C), wollastonite (w), calcium phosphate silicate (Cp) and Apatite (A) are marked.
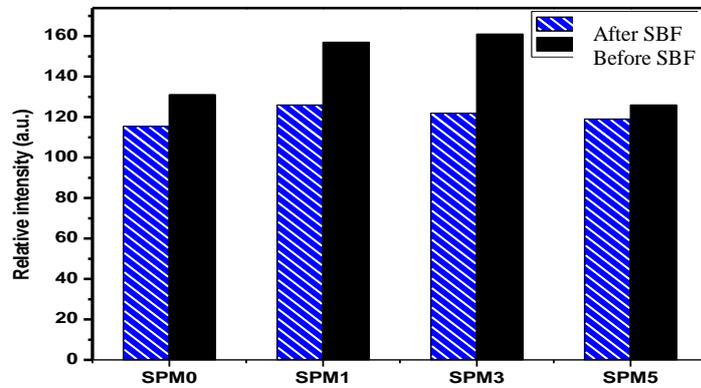
Fig. 7. Comparison between intensity of maximum peak (2 2 0) wollastonite in XRD curves before and after soaking in SBF for all glass-ceramic samples.

Furthermore, the presence of an apatite phase was also observed in all samples, however, the intensity of apatite peaks declined with the increase in MgO content. It seems that the samples apatite-formation ability has some relationship with MgO content which is depends on diopside phase; a higher diopside phase suggests a lower formation rate of apatite.

FTIR analysis

FTIR spectra of glass-ceramics after soaking in the SBF solution were also recorded. After soaking, glass-ceramics SPM$_0$, SPM$_1$ and SPM$_3$ displayed the obvious doublet bands at 606 and 568 cm^{-1} (Fig. 8), which are assigned to crystalline calcium phosphate [32]. However, these above bands, especially band at 606cm^{-1} are not clearly in glass-ceramics SPM$_5$. In addition, the vibration band corresponding to the carbonate groups around at 1438 cm^{-1} were also found in the spectra of all samples after soaking. The appearance of phosphate and carbonate absorption bands in the samples spectra after soaking in SBF not only confirms the formation of an apatite layer but also reveals that the newly formed material is a carbonated hydroxyapatite.

The variation in apatite formation may be due to the difference in the tendency of degradation (dissolution) for the samples with and without magnesium ions contents. However, the degradation of glass-ceramic may be depending on the amount of MgO content which leads to more formation of diopside ceramic phase. The presence of diopside ceramic possessed significantly improved mechanical strength[8], when it compared with wollastonite ceramic, while the degradation rate of the diopside ceramics was extremely low[33]. Therefore, the dissolution rate decreases and chemical durability increases in the samples containing large amount of magnesium containing phase like Diopside,

K. M. TOHAMY *et al.*

resulting in the slower Ca ion release at the first. Also, this fact is related to the preferential association of Mg^{2+} with phosphorus at the glass-ceramic surface. It is worth noting that, the concentration of apatite-like calcium-phosphate domains on the glass-ceramic surface, which is supposed to be the nucleation sites for crystallization of apatite, decreases [34].
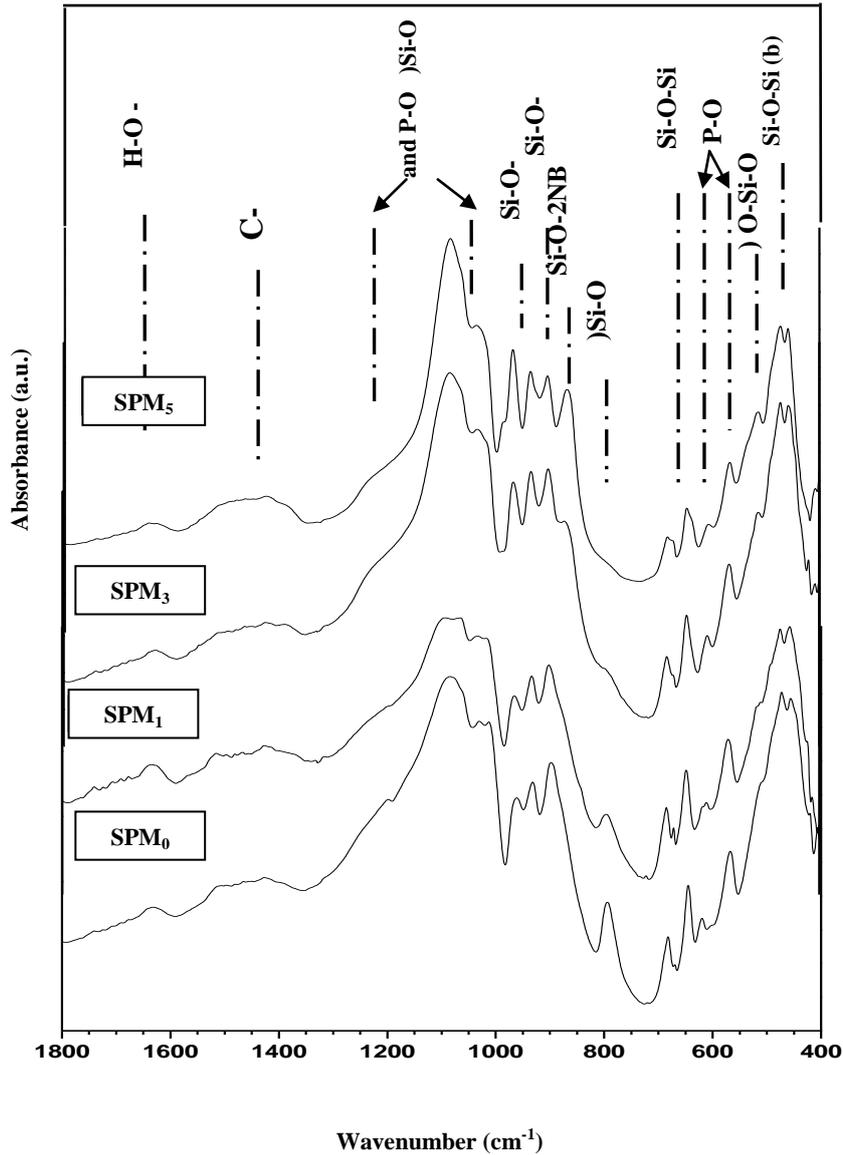

Fig. 8. FTIR spectra for glass-ceramic samples with different additive of MgO content after soaking in SBF for 30 days.

It has been claimed that the content of Mg^{2+} in SBF can highly affect on apatite nucleation which might be the main factor responsible for the decreased carbonated apatite-formation ability**.** These results were consistent with the results of the X-ray analysis of glass-ceramics soaked in SBF andwhich is in a good agreement with previous studies like Ishizawa *et al*.[36]. Finally, although crystallization decreases the samples bioactivity, it does not strictly prevent their apatite-formation ability, even for the glass-ceramics with four crystalline phases. This is due to the presence of crystalline CaSiO$_3$ phase which is regarded as potential bioactive materials for bone tissue regeneration due to their good bioactivity [36].

Conclusion

- Wollastonite, Calcium phosphate silicate and Diopside glass-ceramics were obtained by sintering SiO$_2$–CaO–Na$_2$O–MgO–P$_2$O$_5$ glass system with addition of MgO.

- When MgO content enhanced, the diopside phase formed increased, this led to more durability and the less apatite layer formation in glass-ceramic.

- Less apatite layer formation is due slow rate of ion exchange between surface of sample and solution.

- It possible to design bioactive glass-ceramics system by amount Diopside content which controls the dissolution rate of this system.

References

1. **Hench, L.L., Splinter, R.J., Allen, W.C. and Greenlee, T. K.,** Bonding mechanism at the interface of ceramic prosthetic materails, *J. Bio. Mater. Res.,* **5**, 117-141 (1971).

2. **Blencke, B.A., Bromer, H. and Deutscher, K.K.,** Compatibility and long-term stability of glass ceramic implants, *J. Biomed. Mater. Res*. **12**, 307 (1978) .

3. **Kokubo, T., Ito, S., Sakka, S., Kitsugi, T. and Yamamuro, T.,** Formation of a high-strength bioactive glass-ceramic in the system MgO-CaO-SiO$_2$-P$_2$O$_5$", *J. Mater. Sci.* **21**, 536-540 (1986).

4. **Höland**, **W., Naumann, K. and Vogel, W.** *Machinable, Bioactive Glass Ceramics Materials,* DE 3306648A, pp. 09-22 (1983).

5. **Du**, **R. L., Chang, J. Ni, S.Y., Zhai,W.Y. and Wang, J.Y.** Characterization and *in-vitro* bioactivity of zinc-containing bioactive glass and glass-ceramics, *Journal of biomaterials applications,* **20**, 341–360 (2006).

6. **Szabó, I., Nagy, B., Völksch, G. and Höland, W.,** Structure, chemical durability and microhardness of glass-ceramics containing apatite and leucite crystals", *J. Non-Cryst. Solids,* **272,** 191 (2000).

7. **Martinez, A., Izuierdo-Barba, I. and Vallet-Regi, M.,** Bioactivity of a CaO–SiO$_2$ binary glasses system, *Chem. Mater.* **12**, 3080–3088 (2000).

8. **Vallet-Regi**, **M., Ragel, C.V. and Salinas, A.J.,** Glass with medical application, *Eur. J. Inorg. Chem.* Vol. 1029 (2003).

9. **Wu**, **C.T., Chang, J., Wang, J.Y., Ni, S.Y. and Zhai, W.Y.,** Preparation and characteristics of a calcium magnesium silicate (bredigite) bioactive ceramic, *Biomaterials,* **26**, 2925–2931 (2005).

10. **Xia**, **Wei, Chang, Jiang and Chang,** Preparation and characterization of nano-bioactive-glasses (NBG) by a quick alkali-mediated sol–gel method, *Materials Letters,* **61**, 3251–3253 (2007).

11. **El-Kady**, **Abeer M. , Ali, A.F. Rizk, R.A. and Ahmed Manar, M.** Synthesis, characterization and microbiological response of silver doped bioactive glass nanoparticles, *Ceramics International,* **38**, 177–188 (2012).

12. **Kokubo**, **T. and Takadama, H.** How useful is SBF in predicting *in vivo* bone bioactivity?, *Biomaterials,* **27**, 2907–2915 (2006).

13. **Oki, Aderemi, Parveen, B., Hossain, S., Adeniji, S. and Donahue, H.,** Preparation and *in vitro* bioactivity of zinc containing sol-gel–derived bioglass materials, *J. Biomed Mater Res A*. **69**, 216–21 (2004).

14. **R. Julian Jonesa**, **Ehrenfried, Lisa M. and Hench, Larry L.** Optimising bioactive glass scaffolds for bone tissue engineering, *Biomaterials,* **27**, 964–973 (2006).

15. **Kim, Chang-Yeoul, Jang, A-Rum Kim, Byung-Ik and Dong-Hack Suh,** Surface silylation and pore structure development of silica aerogel composites from colloid and TEOS-based precursor, *J. Sol-Gel Sci Technol,* **48**, 336–343 (2008).

16. **Balkis**, **K. Ameen, K. Rajasekar, Rajasekharan, T. and Rajasekharan, V.** The effect of heat-treatment on the physico-chemical properties of silica aerogel prepared by sub-critical drying technique, *J. Sol-Gel Sci. Technol,* **45**, 9–15 (2008).

17. **Jalota, Sahil Bhaduri, B. Sarit Tas**, **A. Cuneyt** A new rhenanite (β-NaCaPO$_4$) and hydroxyapatite biphasic biomaterial for skeletal repair, *J. Biomed. Mater. Res. Part. B: Appl . Biomater.* B, **80**, 304–316 (2007).

18. **Vallet-Regí, M., Romero, A.M., Ragel, C.V. and LeGeros, R.Z.,** XRD, SEM-EDS and FTIR studies of *in vitro* growth of an apatite-like layer on sol-gel glasses", *J. Biomed. Mater. Res.* **44**, 416-421 (1999).

19. **Balamurugan**, **A., Balossier, G., Kannan, S., Michel, J., Rebelo, A. H.S. and Ferreira, Jose, M.F.** Development and in vitro characterization of sol–gel derived CaO–P$_2$O$_5$–SiO$_2$–ZnO bioglass, *Acta Biomaterialia,* **3**, 255–262 (2007).

20. **Y.J. Park**, **and Bary, P.J.** Determination of the structure of glasses in the manganese borate (MnO–B$_2$O$_3$) system using 11B NMR, *J. Korean Phys. Soc.* **14** (1) 67–74 (1981).

21. **Salman, S.M., Salama, S.N., Darwish, H. and Mahdy, E.A.** The role of MgO on the structural properties of CaO–Na$_2$O(MgO)–P$_2$O$_5$–CaF$_2$–SiO$_2$ derived glass ceramics, *Ceramics International* **36,** 55–61 (2010).

22. **Lefebvre, L., Chevalier, J., Gremillard, L., Zenati, R., Thollet, G., Bernache-Assolant, D. and Govin, A.** Structural transformations of bioactive glass 45S5 with thermal treatments, *Acta Materialia*, **55**, 3305–3313 (2007).

23. **Omori, K.** Analysis of the infrared absorption spectrum of diopside, *The American Mineralogist*, **56**, 1607-1616 (1971).

24. **Kashyap, S., Griep, K. and Nychka, J. A.** Crystallization kinetics, mineralization and crack propagation in partially crystallized bioactive glass 45S5, *Materials Science and Engineering C,* **31**, 762–769 (2011).

25. **Qi-Zhi Chen and Thouas, G.A.** Fabrication and characterization of sol–gel derived 45S5 Bioglass ceramic scaffolds, *Acta Biomaterialia*, **7**, 3616–3626 (2011).

26. **Peitl, O., Oréfice, R.L., Hench, L.L. and Brennan, A.B.** Effect of the crystallization of bioactive glass reinforcing agents on the mechanical properties of polymer composites, *Materials Science and Engineering A,* **372**, 245–251 (2004).

27. **Román, J., Padilla, S. and Vallet-Regí, M.** Sol-Gel Glasses as Precursors of Bioactive Glass-Ceramics, *Chem. Mater.* **15**, 798-806 (2003).

28. **Szumera**, **M., Waclawska, Irene** Spectroscopic and thermal studies of silicate-phosphate glass*, Journal of Thermal Analysis and Calorimetry,* **88** 1, 151–156 (2007).

29. **Lachezar, R., Vladimir, H., Irena M., Maria, H.V.F. and Isabel M. M. S.** *"In vitro* bioactivity of biphasic calcium phosphate silicate glass-ceramic in CaO-SiO$_2$-P$_2$O$_5$ system", *Processing and Application of Ceramics,* **4**(1), 15–24 (2010).

30. **Ma**, **J., Chen, C.Z. Wang, D.G., Shao, X., Wang, C.Z., Zhang, H.M.** Effect of MgO addition on the crystallization and *in vitro* bioactivity of glass ceramics in the CaO-MgO-SiO$_2$-P$_2$O$_5$ system, Ceramics International, **38** (8) 6677–6684(2012).

31. **Ni**, **Siyn, Chang, J. and Chou, L.** "A novel bioactive porous CaSiO$_3$ scaffold for bone tissue engineering", *J. Biomed. Mater. Res. Part A*, **76,** 196–205(2006).

32. **O'Donnell**, **M.D., Watts, S.J., Hill, R.G. and Law, R.V.** The effect of phosphate content on the bioactivity of soda-lime-phosphosilicate glasses, *J. Mater. Sci: Mater Med.* **20,**1611–1618 (2009).

33. **Nonami, T. and Tsutsumi, S.,** Study of diopside ceramics for biomaterials, J. *Mater Sci. Mater. Med.* **10,** 475–479(1999).

34. **Diba**, **Mani Tapia, Felipe and Boccaccini, R. Aldo,** Magnesium-Containing Bioactive Glasses for Biomedical Applications*, International Journal of Applied Glass Science,* **3** (3), 221–253(2012).

35. **Ishizawa, H., Fujino, M. and Ogino, M.** Surface reactions of calcium phosphate ceramics and glass–ceramics to various physiological solutions, *"Handbook of Bioactive Ceramics",* T. Yamamuro, L. L. Hench, and J. Wilson. (Ed.) CRC Press, Boca Raton, FL, 115–123(1990).

36. **Iimory, Kameshima,Y., Okada, K. and Hayashi, S.** Comparative study of apatite formation on $CaSiO_3$ ceramics in simulated body fluids with different carbonate concentrations, *J. Mater. Sci. Mater. Med.* **16,** 73–79 (2005).

تأثير أيون الماغنيسيوم علي تكون طبقة الاباتيت المطعم في الزجاج السيراميكي المحضر بالسول جيل

خيري محمد تهامي، محمد محمود العقر، أشرف فهيم علي*، إسلام سليمان السيد، و محمد إسماعيل الجوهري
قسم الفيزياء – شعبة الفيزياء الحيويه– كلية العلوم (بنين) – جامعة الازهر – مدينة نصر و*قسم الكيمياء الغير عضويه – المركز القومي للبحوث – الدقي – القاهرة – مصر.

تم تحضير الزجاج السيراميكي الحيوي المطعم بالعناصرالقلويه الارضيه بواسطة طريقة السول جيل ذات الوسط القلوي السريع. حيث تم دراسة تأثير تغير اضافة اوكسيد الماغنيسيوم طبقا لنسبة وجود ثاني اوكسيد السيليكون على السلوك الحراري للنظام الزجاجي المكون من $SiO_2–Na_2O–CaO–P_2O_5–MgO$. ومن ثم تم التحقق من هذا النظام الزجاجي بواسطة DSC، TGA، حيود الاشعة السينية و طيف الاشعة تحت الحمراء. بالاضافة إلي ذلك تم دراسة النشاط الحيوي للزجاج السيراميكي خارج الجسم (*in-vitro*) و تم تحليل النشاط الحيوي بواسطة تكون طبقة الاباتيت عند غمر الزجاج السيراميكي في سائل (SBF) مقارب لتركيزات الأملاح الموجودة في بلازما دم الكائن الحي. حيث اوضحت النتائج انه عند المعالجة الحرارية للزجاج الحيوي عند درجة ٩٠٠ مئويه، حيث يتحول الزجاج إلى زجاج سيراميكي ويحتوي على اطوار من البللورات مثل wollastonite, diopside and Calcium phosphate silicate. وعند زيادة تركيز اوكسيد الماغنيسيوم ادي ذلك إلي زيادة تكون نسبة diopsid في الزجاج السيراميكي. كما اظهرت نتائج اختبار الملائمة الحيويه (SBF) ان ترسب طبقة الاباتيت تتناقص بزيادة نسبة وجود طور diopsid في الزجاج السيراميكي. وعلي ذلك يمكن معرفة التحكم في مقدار ترسب طبقة الاباتيت بتحديد نسبة وجود طور diopsid ويمكن تطبيق هذه النتائج عند معالجة كسور العظام وتكون العظام البديلة في الكائنات الحيه.